Memory-efficient 1D Neural Network for PMCW Interference Mitigation in FMCW-based Sensing Systems

Heekwon Yoon, Seonmin Cho, and Seongwook Lee
Department of Electrical and Electronics Engineering
College of ICT Engineering, Chung-Ang University
Seoul, Republic of Korea
{gmlrnjs511, tjsals4514, seongwooklee}@cau.ac.kr

***Abstract*—In this paper, we propose a memory-efficient one-dimensional (1D) neural network to mitigate interference generated by phase-modulated continuous-wave signals in frequency-modulated continuous-wave radar systems. The coexistence of heterogeneous automotive radar systems operating in overlapping frequency bands leads to significant mutual interference. Recently, deep learning-based techniques have been proposed to suppress interference in range-Doppler (RD) maps, owing to their effectiveness in handling complex and diverse interference patterns. However, existing deep learning approaches using two-dimensional (2D) convolutional neural network (CNN) generally process the entire RD map as input, leading to quadratic growth in memory usage as the size of RD map increases. To address this issue, we propose a line-wise processing approach in which each range-bin slice of the RD map is independently restored by a 1D neural network. The proposed architecture maintains nearly constant peak GPU memory (PGM) usage regardless of the size of RD map. Simulation results demonstrate that the proposed model achieves interference suppression performance comparable to a 2D CNN-based method, with an average difference in masked peak signal-to-noise ratio within 0.7 dB. At the same time, the proposed model significantly reduces memory requirements. Specifically, for an RD map of size 256×256, the proposed model reduces PGM usage by 85.89% compared to the 2D CNN-based approach.**

***Index Terms*—Automotive radar, deep learning, frequency-modulated continuous-wave (FMCW), interference suppression, phase-modulated continuous-wave (PMCW).**

I. Introduction

The evolution of autonomous driving systems necessitates not only high-resolution environmental perception but also robust vehicle-to-everything communication capabilities. To address these dual requirements efficiently within constrained resources, integrated sensing and communication (ISAC) systems have emerged as a key solution that integrates both sensing and communication functionalities within a single platform [1]–[3]. Among various waveform candidates for ISAC systems, phase-modulated continuous-wave (PMCW) has been recognized as a promising solution due to its ability to effectively separate sensing and communication signals. However, when PMCW-based ISAC systems are deployed in practical automotive environments, they are likely to coexist with frequency-modulated continuous-wave (FMCW) radars, which are already widely adopted in commercial vehicles. This coexistence of heterogeneous radar systems operating in overlapping frequency bands results in mutual interference [4]. In the FMCW radar receiver, such interference is combined with the desired target echo signals, introducing additional noise-like components that degrade the accuracy of the target detection.

In response to these challenges, deep learning-based interference mitigation techniques have recently gained attention. These approaches are particularly effective in handling complex interference patterns that arise in practical radar systems. Generally, existing deep learning methods directly suppress interference in the range–Doppler (RD) map, enabling effective preservation of target information while mitigating interference [5], [6]. However, directly processing the entire two-dimensional (2D) RD map entails substantial memory consumption, which makes conventional 2D deep learning architectures difficult to deploy on resource-constrained automotive edge hardware. This limitation becomes even more pronounced as modern radar systems increasingly demand larger RD maps (e.g., 2048×2048) for precise sensing. Therefore, this paper proposes a lightweight deep learning-based interference mitigation model that avoids the excessive memory demands of conventional 2D processing. Instead of directly processing the entire 2D RD map, the proposed model decomposes it along the Doppler dimension and independently processes each one-dimensional (1D) range-bin vector using a compact 1D neural network. This line-wise architecture substantially reduces memory consumption while preserving target information, making it well-suited for real-time on-device deployment in automotive radar systems.

II. Signal Model and Interference Analysis

A. Signal Model of Received Signals

An FMCW radar transmits a linear frequency-modulated chirp, which is reflected by the target and received back at the radar. By dechirping the received signal, the resulting baseband

signal at time t can be expressed as

$$\begin{aligned} s_{\mathrm{bb}}(t) = \sum_{n_t=1}^{N_t} & A_r(n_t) \exp\left(j2\pi\left(-K\tau(n_t,\, t)t\right)\right) \\ & \times \exp\left(-j2\pi\left(f_c - \frac{B}{2}\right)\tau(n_t,t)\right) \\ & \times \exp\left(j\pi K\tau(n_t,\, t)^2\right), \end{aligned} \tag{1}$$

where n_t, N_t, $A_r(n_t)$, K, $\tau(n_t,\, t)$, f_c, and B denote the target index, the total number of targets, the amplitude of the received echo from the n_t-th target, the chirp slope, the round-trip propagation delay of the n_t-th target at time t, the center frequency, and the bandwidth, respectively. Here, the round-trip propagation delay is given by

$$\tau(n_t,\, t) = \frac{2(R(n_t) + v(n_t)t)}{c}, \tag{2}$$

where $R(n_t)$, $v(n_t)$, and c denote the range of the n_t-th target, the relative velocity of the n_t-th target, and the speed of light, respectively. In addition,the amplitude of the received echo is derived from the radar equation, which can be expressed as

$$A_r(n_t) = \sqrt{P_t G_t G_r \left(\frac{\lambda}{4\pi R(n_t)}\right)^2 \frac{\sigma}{4\pi R(n_t)^2}}, \tag{3}$$

where P_t, G_t, G_r, λ, and σ denote the power of the transmitted signal, the gain of the transmitting antenna element, the gain of the receiving antenna element, the wavelength, and the radar cross section of the n_t-th target, respectively.

Now, we consider the case where a PMCW interference signal enters the receiver of an FMCW radar system. The received PMCW interference signal with a time delay τ_{I} can be expressed as

$$\begin{aligned} i_{\mathrm{rx}}(t) = A_{\mathrm{I}} \sum_{n_{\mathrm{P}}=0}^{N_{\mathrm{P}}-1} & c_{n_{\mathrm{P}}} \mathrm{rect}\left(\frac{t - n_{\mathrm{P}}T_c - \tau_{\mathrm{I}}}{T_c}\right) \\ & \times \exp\left(j2\pi f_{c,\mathrm{I}}(t - \tau_{\mathrm{I}})\right), \end{aligned} \tag{4}$$

where A_{I}, n_{P}, N_{P}, $c_{n_{\mathrm{P}}}$, T_c, and $f_{c,\mathrm{I}}$ denote the amplitude of the interference signal, the chip index, the total number of chips, the binary phase modulation symbol of the n_{P}-th chip, the chip duration, and the center frequency of the interference signal, respectively. This PMCW interference signal undergoes a dechirping process at the FMCW radar receiver, which includes mixing with the transmitted FMCW signal and subsequent low-pass filtering. This process can be expressed as

$$\begin{aligned} i_{\mathrm{bb}}(t) = & i_{\mathrm{rx}}(t) \\ & \times \exp\left(-j2\pi\left(\left(f_c - \frac{B}{2}\right)t + \frac{K}{2}t^2\right)\right). \end{aligned} \tag{5}$$

The dechirped baseband signal of the PMCW interference can be expressed as

$$\begin{aligned} i_{\mathrm{bb}}(t) = & A_{\mathrm{I}} \sum_{n_{\mathrm{P}}=0}^{N_{\mathrm{P}}-1} c_{n_{\mathrm{P}}} \mathrm{rect}\left(\frac{t - n_{\mathrm{P}}T_c - \tau_{\mathrm{I}}}{T_c}\right) \\ & \times \exp\left(j2\pi\left(f_{c,\mathrm{I}} - f_c + \frac{B}{2}\right)t\right) \\ & \times \exp\left(-j2\pi\left(\frac{K}{2}t^2 + f_{c,\mathrm{I}}\tau_{\mathrm{I}}\right)\right). \end{aligned} \tag{6}$$

Consequently, the total signal at the FMCW radar receiver is the sum of the desired FMCW baseband signal and the dechirped PMCW interference, which can be expressed as

$$s_{\mathrm{mix}}(t) = s_{\mathrm{bb}}(t) + i_{\mathrm{bb}}(t). \tag{7}$$

This signal is then converted into a discrete-time signal using an analog-to-digital converter, which can be expressed as

$$s_{\mathrm{mix}}[n,\, m] = s_{\mathrm{mix}}(t)|_{t=nT_s+mT}, \tag{8}$$

where n, m, T_s, and T denote the fast-time index, the slow-time index, the fast-time sampling interval, and the chirp duration, respectively. Subsequently, a 2D fast Fourier transform is applied to obtain the RD map, which is computed as

$$\begin{aligned} S_{\mathrm{RD}}[r,\, d] = & \sum_{m=0}^{N_c-1} \sum_{n=0}^{N_s-1} s_{\mathrm{mix}}[n,\, m] \\ & \times \exp\left(-j2\pi\left(\frac{nr}{N_s} + \frac{md}{N_c}\right)\right), \end{aligned} \tag{9}$$

where r, d, N_c, and N_s denote the range bin index, the Doppler bin index, the number of chirps per frame, and the number of fast-time samples per chirp, respectively.

B. Impact of PMCW Interference Source on FMCW Receiver

To examine the impact of interference on the RD map, a simple scenario is configured as shown in Fig. 1, where an FMCW radar-equipped vehicle observes two target vehicles. The target vehicles are located at ranges of 50 m and 60 m from the radar-equipped vehicle, with relative velocities of -30 m/s and 10 m/s, respectively. The radar parameters used in this scenario are summarized in Table I. Fig. 2 presents the RD maps generated through the aforementioned signal processing steps. Fig. 2 (a) shows the RD map without interference, where

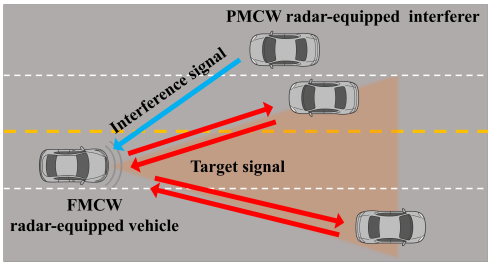

Fig. 1. Scenario for analyzing the impact of PMCW interference on an FMCW radar–equipped vehicle.

TABLE I
SIMULATION PARAMETERS FOR FMCW AND PMCW SYSTEMS

Parameter	FMCW	PMCW
Center frequency	77.125 GHz	77 GHz
Bandwidth	250 MHz	1 GHz
Pulse repetition interval	10 μs	4.09 μs
Number of fast-time samples	256	1023
Number of slow-time samples	256	2503
Sampling duration	39.06 ns	1 ns

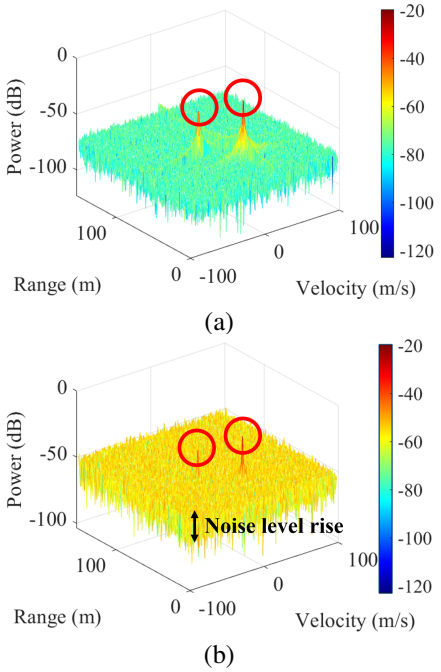

Fig. 2. The RD maps in the FMCW system: (a) without the interference and (b) with the PMCW interference.

the target peaks are clearly distinguishable. In contrast, Fig. 2 (b) shows the RD map with PMCW interference at a signal-to-interference ratio (SIR) of -10 dB. As shown in the figure, the wideband interference elevates the overall noise floor, which degrades the detectability of weak target signals.

III. PROPOSED INTERFERENCE MITIGATION MODEL

To mitigate the PMCW interference, we propose a lightweight 1D convolution neural network (CNN) that independently processes each range line of the RD map. Each input range line of length L is represented by two channels corresponding to the real and imaginary components of the complex-valued signal. The model processes each vector individually to produce a restored output with the same dimensions, and the final reconstructed RD map is obtained by assembling all restored range lines along the Doppler axis.

A. Architecture of Proposed Network

As shown in Fig. 3, the proposed model processes each range line in three main stages. First, an input projection layer expands the channel dimension from 2 (i.e., real and imaginary components) to 64 using a convolution layer (Conv)

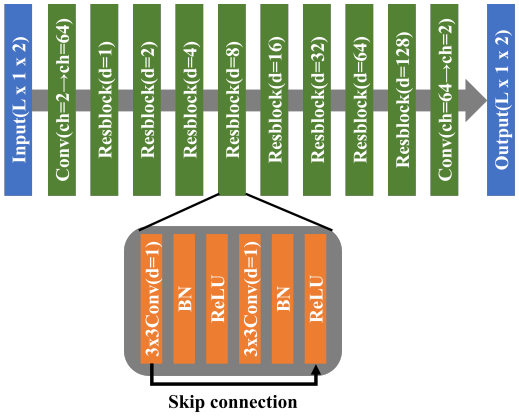

Fig. 3. Architecture of the proposed 1D neural network for interference mitigation.

to effectively represent complex interference patterns through increased feature dimensions. Subsequently, the projected features are processed by a stack of dilated residual blocks (Resblocks), each of which consists of dilated Conv, batch normalization (BN), rectified linear unit (ReLU) activation, and a residual connection. The dilation rate is progressively increased across blocks, enabling the network to extract features over both local and global spatial contexts. Finally, an output projection layer maps the processed features back to the complex-valued domain by reducing the channels to 2.

B. Training and Validation Datasets

To train and evaluate the proposed model, we generate RD map pairs with and without interference using simulations. In each simulation, the number of targets is randomly selected from 1 to 4, and the SIR is randomly selected from the range of -20 dB to 0 dB with a step size of 5 dB. In addition, a total of 1,500 RD map pairs were generated, of which 1,000 pairs were used for training and 500 pairs for validation. In each pair, the interference-contaminated RD map was used as the model input, and the corresponding interference-free RD map was used as the ground truth. Moreover, all RD maps were normalized so that the average noise power equals unity before training. Although the generated RD map has dimensions of $L \times L$, the proposed model processes range line of length L. Therefore, each RD map is decomposed along the Doppler dimension into individual range lines, and each range line is treated as an independent training sample with the real and imaginary components represented as two channels.

C. Configuration of the Proposed Model

The model was trained using the adaptive moment estimation optimizer with a learning rate set to 1×10^{-4}. The variations of the loss values over epochs are presented in Fig. 4. Fig. 4 (a) presents the loss variations with respect to the number of layers, and the lowest loss occurred when the model used eight layers. In addition, Fig. 4 (b) illustrates the loss values for different initial channel counts. An initial channel count of 64 was selected as a suitable configuration, as

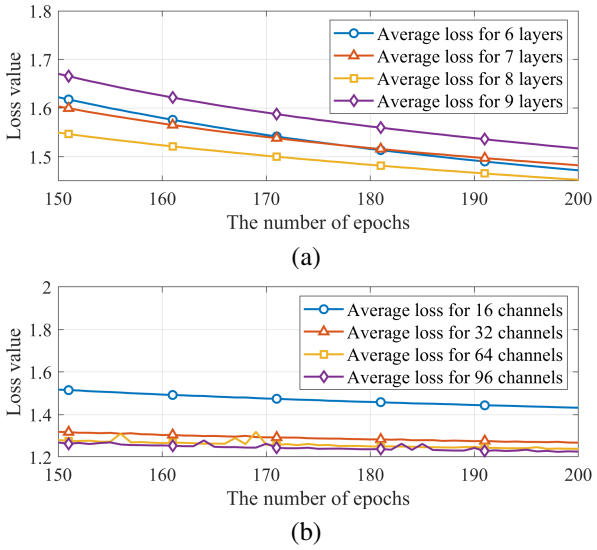

Fig. 4. Training loss curves of the proposed model: (a) different numbers of layers and (b) different numbers of initial channels.

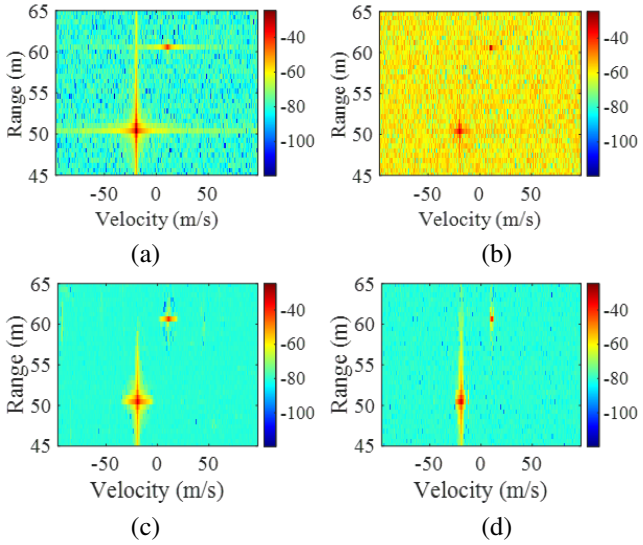

Fig. 5. Reconstructed RD maps for a scenario with two targets: (a) interference-free ground truth, (b) interference-contaminated input, (c) output of the 2D CNN, and (d) output of the proposed model.

further increases yield only marginal performance gains while significantly inflating the computational burden.

IV. Experimental Results and Performance Evaluation

To evaluate the performance of the proposed model, a 2D CNN is used as a baseline for comparison, and both models were trained using identical datasets and training schedules to ensure a fair evaluation [7]. Fig. 5 presents the output results obtained from both models. Fig. 5 (a) shows the interference-free RD map used as the ground truth, and Fig. 5 (b) shows the RD map contaminated by PMCW interference, where the noise floor is significantly elevated. Figs. 5 (c) and (d) show the corresponding outputs generated by the 2D CNN and the proposed model, respectively. As demonstrated in the figures, both models effectively suppress the interference components and restore the target responses.

In addition, two quantitative metrics are used to evaluate restoration performance. The first is the signal-to-interference-plus-noise ratio (SINR), which quantifies the strength of the target responses relative to the residual interference and noise in the reconstructed RD map. The second metric is the masked peak signal-to-noise ratio (mPSNR), which is designed to assess reconstruction accuracy in sparse radar images, where conventional PSNR becomes inadequate due to the dominant contribution of background regions. Let $X(r,\, q)$, $\tilde{X}(r,\, q)$, $\mathcal{T}$, and $\mathcal{B}$ denote the interference-free RD map, the output of the neural network, the set of target bins, and the set of background bins, respectively. The SINR is computed as

$$\mathrm{SINR} = 10\log_{10}\left(\frac{\frac{1}{|\mathcal{T}|}\sum\limits_{(r,\,q)\in\mathcal{T}}|\tilde{X}(r,\,q)|^2}{\frac{1}{|\mathcal{B}|}\sum\limits_{(r,\,q)\in\mathcal{B}}|\tilde{X}(r,\,q)|^2}\right). \tag{10}$$

In addition, to focus on the target region when computing the mPSNR, we consider a 5×5 window $\mathcal{W}$ centered at the point of maximum intensity. The mPSNR is then given by

$$\mathrm{mPSNR} = 10\log_{10}\left(\frac{\frac{1}{|\mathcal{W}|}\sum\limits_{(r,\,q)\in\mathcal{W}}|X(r,\,q)|^2}{\mathrm{MSE}(X,\,\tilde{X})}\right), \tag{11}$$

where $\mathrm{MSE}(X, \tilde{X})$ is the mean squared error between the ground truth and reconstructed RD maps over the entire image. Fig. 6 presents a performance comparison of the two models across various SIR levels, where Figs. 6 (a) and (b) show the resulting SINR and mPSNR, respectively. Both models significantly enhance the SINR and mPSNR across the entire SIR range compared to the interference-contaminated input, demonstrating effective suppression of PMCW interference. In terms of averaged performance, the proposed model achieves an SINR improvement of 19.61 dB and an mPSNR gain of 22.22 dB, and the 2D CNN achieves corresponding improvements of 18.61 dB and 22.92 dB, respectively. These results indicate that the proposed 1D model provides interference sup-

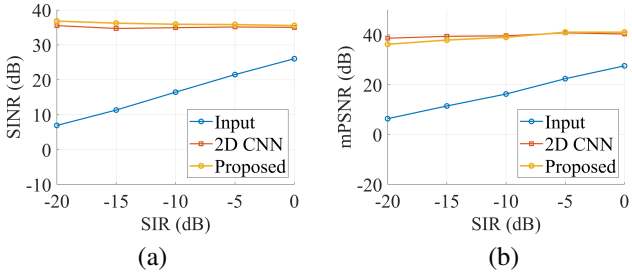

Fig. 6. Quantitative evaluation of interference suppression performance versus input SIR: (a) SINR and (b) mPSNR.

pression performance comparable to that of the conventional 2D CNN.

Meanwhile, Table II summarizes the computational complexity of both models, evaluated in terms of the number of parameters and floating-point operations (FLOPs). The 2D CNN requires 224.71 K parameters and 29.49 GFLOPs per frame, and the proposed model reduces these values to 198.47 K parameters and 25.87 GFLOPs per frame. The reported FLOPs correspond to the number of operations needed to process a single RD frame of size 256×256. In addition, Fig. 7 presents the peak GPU memory (PGM) as a function of the input size of RD map. PGM is a critical metric for on-device deployment, because embedded hardware has strict memory constraints and an out-of-memory failure occurs when the PGM exceeds the available memory [8]. As shown in Fig. 7, unlike conventional 2D CNN whose PGM grows rapidly with input size of RD map, the proposed 1D line-wise model maintains an extremely low and stable memory requirement. This behavior originates from the structural property of the 1D architecture, which processes each range line independently rather than loading the entire 2D RD map into memory. As a result, the PGM depends only on the line length and remains nearly unchanged even when the RD size increases. For example, when the size of RD map increases from 256×256 to 2048×2048, the PGM of the 2D CNN expands from 50.01 MB to more than 2.42 GB. Such a dramatic increase reflects the inherent limitation of 2D CNN, which requires the storage of large intermediate activation tensors that span the entire spatial dimension. In contrast, the proposed model requires only 7.06 MB to 13.74 MB. This characteristic makes the proposed model particularly suitable for high-resolution imaging radars, where memory availability is often the primary bottleneck. In summary, the results in Table II and Fig. 7 confirm the low computational complexity and strong memory scalability of the proposed architecture. These characteristics are essential for a hardware-friendly deployment in practical automotive radar systems.

TABLE II
COMPUTATIONAL COMPLEXITY COMPARISON BETWEEN THE 2D CNN AND THE PROPOSED MODEL

Metric	2D CNN	Proposed model
Parameters	224.71 K	198.47 K
FLOPs per frame	29.49 GFLOPs	25.87 GFLOPs

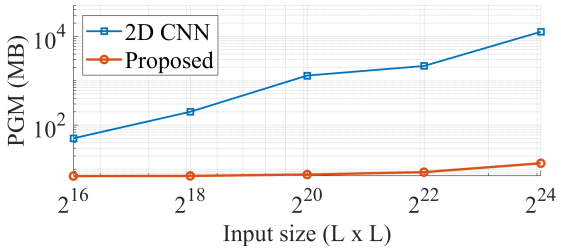

Fig. 7. PGM consumption as a function of size of RD map ($L \times L$).

V. CONCLUSION

This paper proposed a memory-efficient interference mitigation model for FMCW radar systems affected by PMCW interference. First, we constructed a scenario in which an FMCW radar operates in the presence of a coexisting PMCW radar and analyzed the resulting distortion in the RD map caused by mutual interference. The analysis confirmed that wideband PMCW interference elevates the noise floor and significantly degrades the visibility of weak target signals. To address this issue, we introduced a lightweight model designed to restore RD maps corrupted by interference. Unlike conventional 2D approaches that process the entire RD map simultaneously, the proposed model processes each range line of the RD map independently, resulting in substantially reduced memory requirements. Specifically, when processing RD maps of size 256×256, the proposed model reduced PGM usage by 85.89% compared with the 2D CNN architecture. In addition, the proposed model achieved interference suppression performance comparable to that of the 2D CNN in terms of SINR and mPSNR. These results suggest that the proposed model can offer advantages for deployment on embedded automotive radar platforms operating under strict memory and power constraints.

ACKNOWLEDGMENT

This work was supported by the National Research Foundation of Korea (NRF) grant funded by the Korea government (MSIT) (No. RS-2024-00405510).

REFERENCES

[1] C. Park, S. Lee, and T. Jeong, "High-resolution ranging scheme for stepped-frequency PMCW-based ISAC systems," *2025 IEEE VTS Asia Pacific Wireless Communications Symposium (APWCS)*, Tokyo, Japan, August 2025, pp. 1–3.

[2] Y. Choi, C. Park, J.-H. Lee, and S. Lee, "ConvLSTM Autoencoder-based CSI prediction for efficient target detection in TDD-based OFDM ISAC systems," *IEEE Internet of Things Journal*, early access, 2025, doi: 10.1109/JIOT.2025.3639084.

[3] C. Park, J.-H. Park, T. Jeong, J. Joung, and S. Lee, "Efficient frame structure design of PMCW radar based on Golay sequence in 802.11ad preamble," *IEEE Internet of Things Journal*, vol. 12, no. 24, pp. 53177–53189, December 2025.

[4] L. A. López-Valcárcel and M. G. Sánchez, "Study of the mutual interference between FMCW and PMCW automotive radars," *2025 IEEE Radar Conference (RadarConf25)*, Krakow, Poland, October 2025, pp. 1629–1634.

[5] H.-W. Hsu, Y.-C. Lin, M.-C. Lee, C.-H. Lin, and T.-S. Lee, "Deep learning-based range-Doppler map reconstruction in automotive radar systems," *2021 IEEE 93rd Vehicular Technology Conference (VTC2021-Spring)*, Helsinki, Finland, May 2021, pp. 1–7.

[6] A. A. ElSharkawy, A. S. Abdallah, and M. W. Fakhr, "A new semantic segmentation technique for interference mitigation in automotive radar," *2023 IEEE Wireless Communications and Networking Conference (WCNC)*, Glasgow, United Kingdom, March 2023, pp. 1–6.

[7] J. Rock, M. Toth, E. Messner, P. Meissner, and F. Pernkopf, "Complex signal denoising and interference mitigation for automotive radar using convolutional neural networks," *2019 22nd International Conference on Information Fusion (FUSION)*, Ottawa, Ontario, Canada, July 2019, pp. 1–8.

[8] Z. Li, A. Samanta, Y. Li, A. Soltoggio, H. Kim, and C. Liu, "R^3: On-device real-time deep reinforcement learning for autonomous robotics," *2023 IEEE Real-Time Systems Symposium (RTSS)*, Taipei, Taiwan, December 2023, pp. 131–144.